Journal of Alloys and Compounds 505 (2010) 486–491

Contents lists available at ScienceDirect

Journal of Alloys and Compounds

journal homepage: www.elsevier.com/locate/jallcom

Microindentation of dispersed phases in an $Al_{94}Mn_2Be_2Cu_2$ alloy

Tonica Bončina [a], Miha Čekada [b], Boštjan Markoli [c], Franc Zupanič [a,*]

[a] University of Maribor, Faculty of Mechanical Engineering, Smetanova 17, SI-2000 Maribor, Slovenia
[b] Jožef Stefan Institute, Jamova 39, SI-1000 Ljubljana, Slovenia
[c] University of Ljubljana, Faculty of Natural Sciences and Engineering, Askerceva 12, SI-1000 Ljubljana, Slovenia

ARTICLE INFO

Article history:
Received 27 April 2010
Received in revised form 14 June 2010
Accepted 16 June 2010
Available online 25 June 2010

Keywords:
Metals and alloys
Quasicrystals
Intermetallics
Elasticity
Mechanical properties
Scanning electron microscopy

ABSTRACT

This paper investigated properties of dispersed phases in an $Al_{94}Mn_2Be_2Cu_2$ alloy using a microindentation hardness test. The focus was directed to the possible strengthening phases for aluminium alloys: an icosahedral quasicrystalline phase (i-phase), a hexagonal quasicrystalline approximant with a large unit cell (H-phase) and a ternary cubic Be_4AlMn. A single grain μ-Al_4Mn was also examined as a reference. The application of scanning electron microscopy and a focussed ion beam, significantly increased the reliability and reproducibility of the microindentation results. The i-phase was distinguished by the highest Vickers hardness and the highest fraction of elastic energy, while the elastic modulus was the highest for Be_4AlMn, being close to that of pure Be. The striking resemblances of the indentation curves for the phases with cluster substructures: i-phase, H-phase and μ-Al_4Mn, especially the presence of pop-ins, suggested related deformation mechanisms.

1. Introduction

Over recent years, microindentation hardness tests have been utilized more frequently than ever for measuring the mechanical properties of various materials – ranging from ductile metals to brittle ceramics [1–4], as well as for bones [5] and tooth enamel [6]. This can be attributed to the ease and speed with which they can be conducted, nondestructiveness, the ease of testing under special conditions and, finally, offering the possibility of greatly reducing the scale of the tests. However, the reduction in indent size gives rise to several effects influencing evaluation of the results using microindentation. Firstly, indents can become too small to be clearly resolved under an optical microscope being an essential part of the microindentation instrumentation, requiring subsequent examination under a scanning electron microscope for determining their shapes and possible pile-ups, or performing the indentation tests in an atomic force microscope [7]. Secondly, the influence of surface conditions (roughness, mechanical deformation) increases with decreasing indent size necessitating the optimised sample preparation [8]. Last, but not least, the indentation size effect (ISE), which is defined as the increase in hardness with decreasing indent size needs to be taken into account. The comprehensive review of its origin was given by Mukhopadhyay and Paufler [9].

Over the recent years several reports have been published regarding indentation hardness tests on stable quasicrystals [7,10,11]. On the other hand, no reports can be found about the indentation hardness of metastable quasicrystals. Namely, small particle sizes in rapidly solidified alloys prevent the hardness measurements of individual particles. Improvement in the quasicrystal forming abilities of some aluminium alloys have given rise to the formation of metastable quasicrystals at much smaller cooling rates attainable by conventional casting [12]. Consequently, quasicrystalline particles are considerably larger due to noticeably lower cooling rates, making indentation hardness measurements feasible. In addition to quasicrystals, determining the mechanical properties of quasicrystalline approximants has become a very important issue [13]. Quasicrystalline approximants possess very large unit cells containing up to thousands of atoms. Both quasicrystals and quasicrystalline approximants consist of well-defined clusters, most often of icosahedral symmetry, and belong to a class of so-called complex metallic alloys [14]. In one of the recently developed alloys, an $Al_{94}Mn_2Be_2Cu_2$ alloy [15], both an i-phase and a quasicrystalline approximant can be found. This offers a nice possibility of making comparison between the mechanical properties of these two phases, having very similar compositions and cluster arrangements. Indentation hardness tests were also carried out on Be_4AlMn (fcc, $a = 0.611$ nm, cF24 [16]) and the single crystalline μ-Al_4Mn ($a = 1.9980$ nm, $c = 2.4673$ nm, hP574, $P6_3/mmc$ [17]), which is closely related to the quasicrystalline approximant present in $Al_{94}Mn_2Be_2Cu_2$. In addition, all of these phases can contribute to the strengthening of aluminium alloys; representing another reason for investigating their mechanical properties. Dispersed phases and small particle sizes called for small loads during microindentation testing, often causing a significant mismatch of

* Corresponding author. Tel.: +386 2 220 7863; fax: +386 2 220 7990.
E-mail address: franc.zupanic@uni-mb.si (F. Zupanič).

0925-8388/$ – see front matter © 2010 Elsevier B.V. All rights reserved.
doi:10.1016/j.jallcom.2010.06.111

hardness values. Thus a combined approach to using microindentation and microscopy (SEM and focussed ion beam, FIB) was chosen to increase the reliability and reduce the scattering of the results.

2. Materials and methods

The indentation study was performed on an $Al_{94}Mn_2Be_2Cu_2$ (at.%) alloy, and a single crystalline μ-Al_4Mn ($Al_{79.3}Mn_{20.7}$); more details about the latter phase can be found in Ref. [18]. The $Al_{94}Mn_2Be_2Cu_2$ alloy was vacuum induction melted and die-cast into cylindrical copper moulds with diameters of 3 mm and 50 mm. The samples were investigated using SEM (Sirion 400 NC, FEI) equipped with EDS (Inca 350, Oxford Instruments), XRD (synchrotron radiation, λ = 0.1 nm, Sincrotrone Elettra, Trieste, Italy) and Tof SIMS (time-of-flight secondary ion mass spectroscopy, Cameca TOF-IV).

The samples were prepared using typical mechanical metallographic preparation techniques. The final stage consisted of polishing with 1 μm diamond paste. The indentation hardness tests were carried out on a Fisherscope H100C testing machine (Fisher Technology). The loading and unloading times were 10 s each. The maximum loads applied ranged from 5 mN to 500 mN. After the tests, the Martens hardness *HM*, the Vickers indentation hardness *HV*, reduced elastic modulus E_r and, the fraction of elastic energy η_{IT} were evaluated according to the standard EN ISO 14577 [19]. Indents were observed in SEM and, in some cases milled using focussed ion beam FIB (Quanta 200 3D, FEI) in order to determine the shapes of the indents, thicknesses of the investigated particles, and the presence of any cracks under the indents.

3. Results and discussion

3.1. Microstructure of the investigated alloys

Fig. 1 shows the microstructures of the investigated alloy under two as-cast conditions. The alloy $Al_{94}Mn_2Be_2Cu_2$ cast into the 50 mm diameter cylindrical mould consisted of five phases: hexagonal H-phase, cubic Be_4AlMn, Θ-Al_2Cu, τ_1-$Al_{29}Mn_6Cu_4$ and Al-rich matrix (Fig. 1a). The EDS results indicated the atomic ratio Al:Mn = 4:1 for the hexagonal H-phase, which is almost the same as in μ-Al_4Mn. However, the H-phase also contained about 2 at.% Cu (EDS) and perhaps 2–5 at.% Be, estimated on the basis of a qualitative ToF SIMS investigation. XRD revealed the presence of a hexagonal phase with lattice parameters of $a = 1.22736$ and $c = 2.45396$, similar to those found in Al–Mn–Be alloys by Kim et al. [12]. Be_4AlMn dissolved a small amount of Cu, and the lattice parameter $a = 0.612$ nm was almost the same as in pure Be_4AlMn. The lattice parameters of orthorhombic τ_1 were $a = 2.421$ nm, $b = 0.772$ nm and $c = 1.249$ nm, and those of tetragonal Θ-Al_2Cu: $a = 0.606$ nm and $c = 0.486$ nm. The samples cast into the cylindrical 3 mm mould were composed of only three phases: icosahedral quasicrystalline phase (i-phase, a quasilattice constant of $a = 0.46$ nm), tetragonal Θ-Al_2Cu ($a = 0.605$ nm, $c = 0.484$ nm) and a fcc Al-rich solid solution ($a = 0.404$ nm) (Fig. 1b). The Al to Mn ratio in the i-phase was almost the same as in the H-phase, but it contained a much higher amount of Be (30%), and approximately 2 at.% Cu. The indentation hardness tests were carried on three phases Be_4AlMn, H-phase, and the i-phase. The main aim was to study those phases with great differences in their structures. Be_4AlMn has a relatively small number of atoms in the unit cell (24 atoms) and can be classified as a simple intermetallic phase. In contrast, the H-phase belongs to a group of complex metallic alloys, having large unit cells with large cluster-like building blocks, alike to those found in quasicrystalline phases. Finally, the i-phase is quasiperiodic (infinite unit cell), belonging to the Mackay-type of quasicrystals. Typical sizes of particular phases and critical loads for initiating cracks around the indents are given in Table 1.

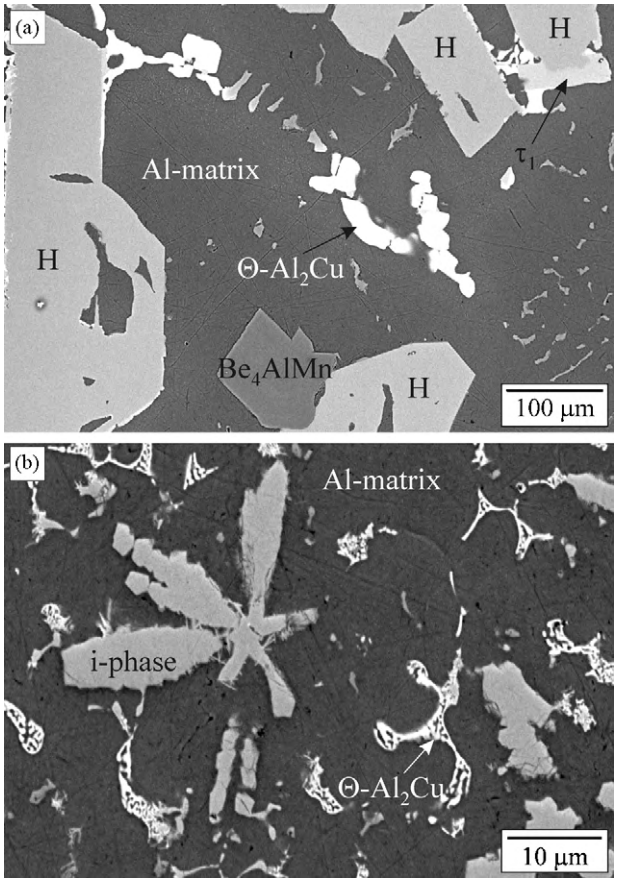

Fig. 1. Backscattered electron micrographs of the alloy $Al_{94}Mn_2Be_2Cu_2$ (a) cast into the 50 mm copper mould and (b) die-cast into the 3 mm copper mould.

Table 1
Size ranges of the investigated phases and the critical loads initiating cracks around indents.

Phase	H-phase	Be_4AlMn	i-Phase
Size of particles (μm)	Up to 250	Up to 50	Up to 20
Critical load (mN)	500	200	30

3.2. Selection of measurements for evaluating the results

The small sizes of most particles required the application of small loads, often causing large mismatches of the results. In order to increase the reliability and to reduce the scattering of the results, each indent and indentation curve was closely inspected. A load significantly exceeding the critical load gave rise to a complete fracture of the investigated particle, which could be easily observed under a light microscope. In a loading curve, very large pop-ins (discontinuities in the load–displacement curve) in the order of 50–100 nm sometimes appeared (Fig. 2a), despite the fact that no cracks formed around an indent. In such a case, ion-milled cross section regularly revealed the presence of several cracks beneath the indent (Fig. 2b) or the very small thickness of a particle. This could also be inferred from the much smaller values for hardness and reduced modulus (*HV* = 4.2 GPa and $E_r = 24$ GPa, in comparison with *HV* = 14 GPa and $E_r = 151$ GPa).

Contrary to the previous case, the indentation curve in Fig. 3a shows no large pop-ins, yet the modulus of elasticity and hardness deviated far too much from the average values. SEM inspection showed the presence of rather large cracks, and the too small a distance of the indent from the neighbouring phase (Fig. 3b).

Based on careful observations of the indents and indentation curves, a measurement was not included in the evaluation when at least one of the following criteria was fulfilled:

- The hardness values or modulus of elasticity were much smaller than the average values.
- The indent was too close to the edge of a particle.

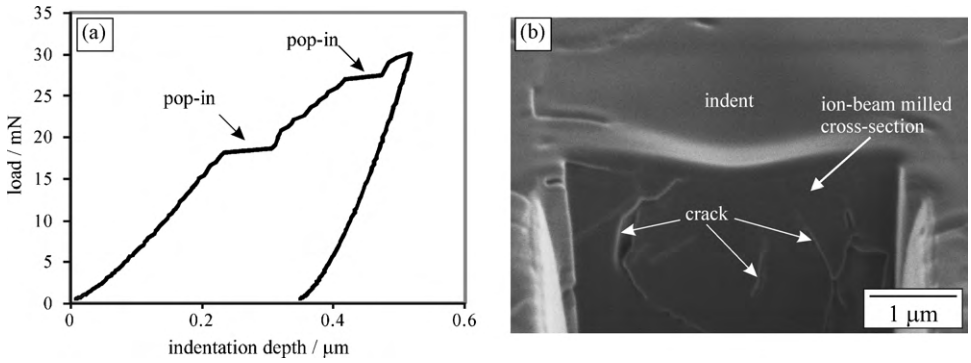

Fig. 2. Indentation test on an i-phase particle (F = 30 mN). The pop-ins on the loading curve (a) appeared due to formation of the crack network below the indent as revealed on the ion-milled cross section.

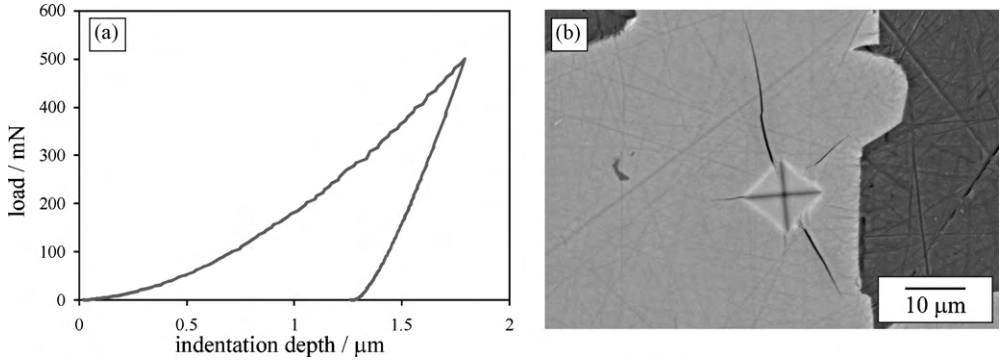

Fig. 3. Indentation test on a particle of H-phase (F = 500 mN). (a) Indentation curve without pop-ins (HV = 6.61 GPa and E_r = 155 GPa) and (b) long cracks emerging from the indent (BSE).

- The large pop-ins were observed on the indentation curve.
- The indentation depth approached or exceeded the thickness of a particle.
- Cracks were observed around indents.

Fig. 4 shows two indents lying on the borderline between accepted and rejected measurements. They were accepted, even though they were very close to the particle edges (around 1d). However, there were no cracks, the indentation curve was smooth without large pop-ins and the measured values did not deviate from the values obtained when the distances from the edges were greater.

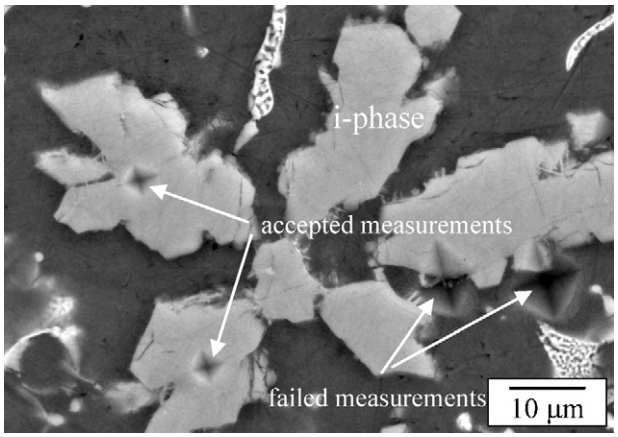

Fig. 4. An example of accepted measurements: two indents in the i-phase of $Al_{94}Mn_2Be_2Cu_2$ after casting into the 3 mm copper mould.

3.3. Properties of phases

Fig. 5 comprises the Vickers hardness HV for all investigated phases as a function of load F. The scattering of the results for loads of 5 mN and 10 mN was very large, therefore those values were not included in the diagram, except for μ-Al_4Mn. This could be mainly attributable to extrinsic factors such as vibrations and sur-

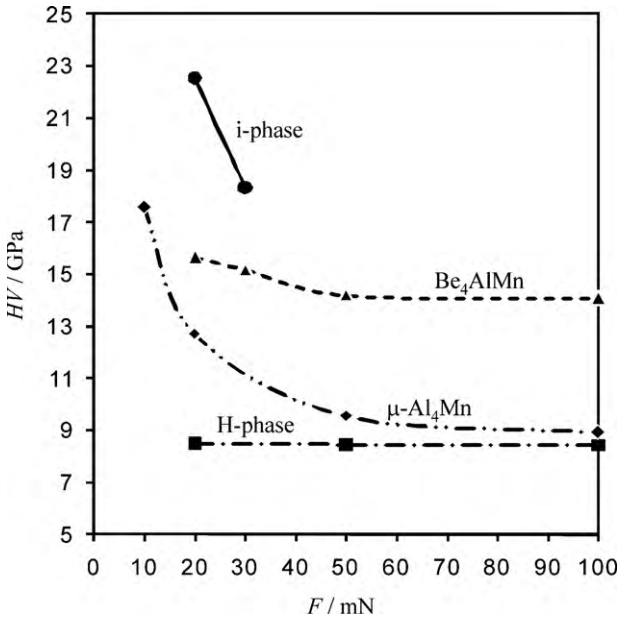

Fig. 5. The average Vickers hardness of the investigated phases as a function of load F.

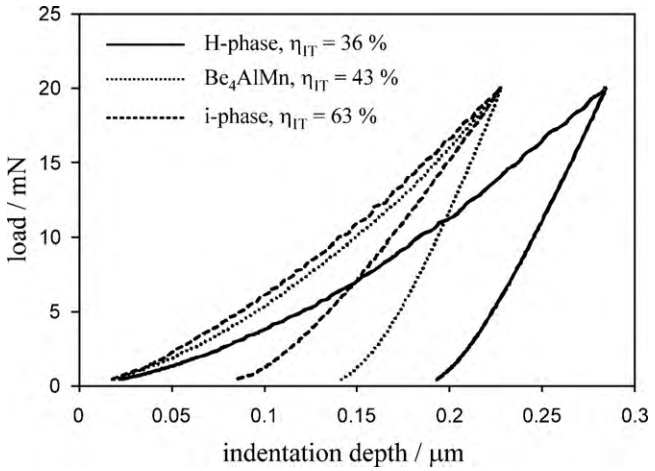

Fig. 6. Indentation curves for the investigated phases in the $Al_{94}Mn_2Be_2Cu_2$ alloy using a load of 20 mN.

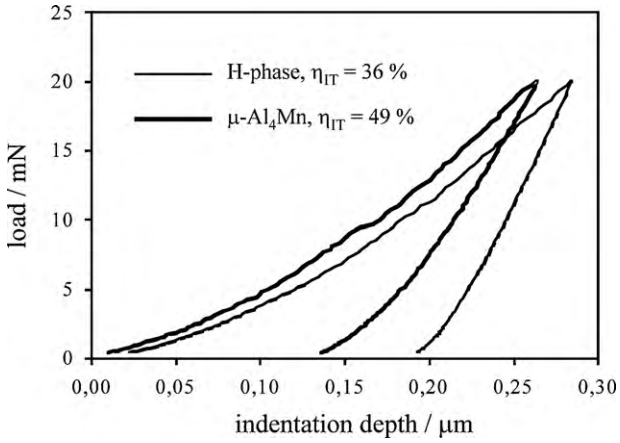

Fig. 7. The indentation curves of μ-Al_4Mn and H-phase using a load of 20 mN.

face roughness. The H-phase did not exhibit any ISE, while the effect of ISE in Be_4AlMn was rather weak. Conversely, this effect was much more pronounced for the i-phase and μ-Al_4Mn. Similar behaviour can be found in other systems, for example, Mukhopadhyay et al. reported strong ISE for an Al–Ni–Co decagonal quasicrystal [10], but absence of ISE for Zn–Mg–Er and Zn–Mg–Ho icosahedral phases [7]. The small size, dendritic shape and presumably high concentration of defects in the i-phase probably caused the inhomogeneous stress state with high local stress concentrations, leading to fracturing at relatively small loads, and prevented the application of loads higher than $F > 30$ mN.

Fig. 6 shows the typical indentation curves of the selected phases and Table 2 summarises the results. The indentation curves of Be_4AlMn were rather smooth; the depth of the indent monotonously increased with increasing load, which is also typical for simple metals; such as Al [11]. On the other hand, the indentation curves of the i-phase were characterized by a series of small pop-ins, and the same features could also be observed on the indentation curves of quasicrystalline approximants H-phase and μ-Al_4Mn (Fig. 7), thus sharing similar cluster substructure [12,17]. The hardness values of the i-phase, especially the Vickers hardness, strongly exceeded the hardness values of other phases. This could be attributed to the fact that its quasiperiodic structure offered much greater resistance to plastic deformation than the periodic structures of quasicrystalline approximants (H-phase), which was also found in other investigations [1].

The reduced modulus of the i-phase was 160 ± 10 GPa, and those of the H-phase and μ-Al_4Mn were almost the same 175 ± 8 GPa (Table 2). On the other hand, Be_4AlMn exhibited much higher E_r in the order of 250 ± 10 GPa. Using the appropriate elastic constants for the Vickers indenter ($G = 1140$ GPa, $\nu = 0.07$) and the Poisson's ratio of 0.23 [7] for the i-phase and 0.3 for the other phases, the average E values turned out to be 187 GPa, 188 GPa, 182 GPa and 295 GPa for the i-phase, H-phase, μ-Al_4Mn and Be_4AlMn, respectively. It should be noted that the Poisson's ratios of the present phases are unknown. However, typical values for intermetallic phases are around 0.3. By taking Poisson's ratios between 0.25 and 0.35, the results deviated by only ±5% from the calculated E. This is within the experimental precision of the measurements. The elastic modulus reflects the strength of interatomic bonding. Thus, the strength of the interatomic bonding was almost the same as for i-phase, H-phase and μ-Al_4Mn; i.e. the phases with the substructures made of Mackay clusters, despite some differences in their chemical compositions, periodicities, and sizes of their unit cells. The modulus of elasticity for the i-phase was comparable to those of other aluminium quasicrystals (Table 3). Interestingly, the elastic modulus of Be_4AlMn almost completely matched that of pure Be, indicating that the Be–Be interactions had a dominant influence on its elastic properties.

The Martens hardness is the resistance of a material against both elastic and plastic deformation. It was calculated under the maximum load. The highest values were attained by the i-phase and Be_4AlMn (≈9 GPa), whereas the values for the Martens hardness were much lower for the H-phase and μ-Al_4Mn. The permanent deformation of the i-phase was much smaller than those of the other phases due to its higher fraction of elastic energy (>60%). This resulted in a much higher Vickers hardness, which reflects the nature of resistance to plastic deformation. At 20 mN the Vickers hardness of the i-phase strongly exceeded the hardnesses of other phases, indicating that its quasiperiodic structure offered much greater resistance than the periodic structures of quasicrystalline approximants. It should be stressed that even the hardness of the softest H-phase attained a value comparable to the top hardness of hardened steel (≈800 HV). The hardness values of other Al-quasicrystals are available at relatively higher loads (see Table 2 and Ref. [9]); therefore a direct comparison with the current values was impossible because of ISE. For this reason, hardness measurements were additionally carried out at 20 mN and 30 mN on the i-phase, in an $Al_{64}Cu_{23}Fe_{13}$ alloy. It was revealed that, at these loads, the hardness of the i-phase in $Al_{94}Mn_2Be_2Cu_2$ was approximately ≈50% higher than the hardness of i-phase in $Al_{64}Cu_{23}Fe_{13}$. If this ratio were to be also valid for higher loads, then hardness levels up to 1.5 GPa would be expected, making the i-phase in $Al_{94}Mn_2Be_2Cu_2$ a promising hardening phase. The properties of the μ-Al_4Mn and H-phases did not differ a lot. This could be inferred from their structural resemblance [12,17]. The higher values for μ-

Table 2
Properties of the investigated phases in the $Al_{94}Mn_2Be_2Cu_2$ alloy and μ-Al_4Mn determined using the microindentation test at an applied load of 20 mN.

	Alloy	*HM* (GPa)	*HV* (GPa)	E_r (GPa)	*E* (GPa)	η_{IT} (%)
i-Phase	$Al_{94}Mn_2Be_2Cu_2$	8.8 ± 0.5	22.5 ± 2.0	161 ± 9	177	63 ± 3
H-phase	$Al_{94}Mn_2Be_2Cu_2$	6.1 ± 0.24	8.1 ± 0.35	175 ± 6	188	36 ± 2
Be_4AlMn	$Al_{94}Mn_2Be_2Cu_2$	9.1 ± 0.1	13.4 ± 0.2	253 ± 8	295	43 ± 2
μ-Al_4Mn	$Al_{79.3}Mn_{20.7}$	7.5 ± 0.1	12.9 ± 0.2	172 ± 8	182	49 ± 2

Table 3
Properties of selected phases, determined by indentation hardness testing.

Phase or alloy	F (mN)	HV (GPa)	HV/E	E (GPa)	Source
Single crystalline i-phase	500	10.4	0.06	167	[21]
$Al_{62}Cu_{25.5}Fe_{12.5}$	2000	8.7			
	5000	8.1			
Polycrystalline i-phase	500	7.85 ± 0.60	0.047	167	[20]
$Al_{62.5}Cu_{24.0}Fe_{12.5}$	5000				
Polycrystalline i-phase	–	9.95 ± 1.0	0.089	112	[22]
$Al_{64}Cu_{22}Fe_{14}$					
Polycrystalline i-phase	–	7.19	–	–	[23]
$Al_{65}Cu_{20}Fe_{15}$					
Polycrystalline i-phase		7.62	–	–	[23]
$Al_{50}Cu_{20}Fe_{15}Si_{15}$					
Single crystalline i-phase Zn–Mg–Er	16	8.5 ± 0.2	0.06	140 ± 10	[7]
Single crystalline i-phase Zn–Mg–Ho	16	8.5 ± 0.2	0.055	140 ± 10	[7]
$Cu_{47}Ti_{33}Zr_{11}Ni_6Sn_2Si_1$ metallic glass	16	7.8 ± 0.1	0.05	125 ± 5	[24]
$Al_{63}Si_2Cu_{20}Co_{15}$	15	9.01 ± 0.33	0.05	181 ± 5	[25]
	500	8.24 ± 0.16			

Al_4Mn may arise from its higher structural perfection because it was held for a long time at high temperatures during single crystal growth, whereas the H-phase formed during solidification with an approximate cooling rate of 10 K/s.

In spite of several investigations, there is still a lack of agreement regarding the plastic deformation of quasicrystalline phases at low temperatures. Quasicrystalline phases and intermetallic compounds share a homologous brittle-to-ductile transition temperature of $T/T_m \approx 0.7$ (T_m – melting temperature) [20], thus diffusion processes which are non-viable at room temperature are strongly involved in plastic deformation. However, indentation experiments are performed under confined pressure conditions, where uniaxial stress states are superimposed by hydrostatic pressure, the BDT can be lowered down to room temperature by suppressing crack growth. High hydrostatic pressure can allow for dislocation glide and multiplication in Be_4AlMn, similar to the deformation mechanism in simple metals, resulting in a monotonically increasing indentation curve.

The close resemblances of indentation curves for the i-phase, H-phase and μ-Al_4Mn, especially the presence of pop-ins, can lead to the conclusion of related deformation mechanisms in all phases. It should be taken into account each has a similar cluster substructure, and very likely exhibits the same strain softening as other quasicrystals and quasicrystalline approximants. Deformation mechanisms have normally been studied on single grained specimens. Yet, the i-phase in the investigated alloy is metastable and cannot be grown as a single crystal. Quasicrystalline phases can deform via dislocation glide and climb at higher temperatures. On the other hand, plastic deformation in complex metallic alloys with very large unit cells was found to be mediated by metadislocations. The glide of a metadislocation inevitably involves local phase transformation to a closely related structure [13]. Very high brittle-to-ductile transition temperatures very likely cause the absence of active dislocations in the i-phase, and metadislocations in the H-phase and μ-Al_4Mn, at room temperature. Recently, Mukhopadhyay et al. [7] revealed the formation of shear bands in a step-wise manner by using atomic force microscopy. They concluded that this could be the initial mechanism for plastic deformation and can be related to pop-ins. In subsequent stages it can be followed to phase transformation in a softer periodic quasicrystalline approximant. These two-step processes appeared more feasible than the direct quasicrystal-to-crystal transition proposed by Dub et al. [11]. The deformation through formation and propagation of shear bands could also be a viable mechanism for plastic deformation of approximant phases as well. Nevertheless, it seems that the explanation for plastic deformation mechanisms in phases with large unit cells requires further detailed investigations.

4. Conclusions

The results of our work lead us to the following conclusions.

The H-phase did not exhibit any ISE, while the effect of ISE in Be_4AlMn was rather weak. Conversely, this effect was much more pronounced for the i-phase and μ-Al_4Mn. The very low critical load for the formation of cracks in the i-phase and the small sizes of i-phase particles prevented the application of loads higher than $F > 30$ mN.

The average E values for the i-phase, H-phase, μ-Al_4Mn, and Be_4AlMn turned out to be 187 GPa, 188 GPa, 182 GPa and 295 GPa, respectively. This inferred similar strengths for interatomic bonding regarding the i-phase, H-phase, and μ-Al_4Mn; i.e. those phases with resembling cluster substructures. The elastic modulus of Be_4AlMn almost completely matched that of pure Be, indicating that the Be–Be interactions had a dominant influence on its elastic properties.

The close resemblance of indentation curves for the i-phase, H-phase and μ-Al_4Mn, especially the presence of pop-ins, can lead to the conclusion of related deformation mechanisms in all phases. The i-phase was distinguishable from the other phases by its higher fraction of the elastic energy (>60%), and a much higher hardness at 20 mN (>2.2 GPa), making this phase an interesting hardening phase for Al-alloys.

Acknowledgements

We would like to thank Dr. Peter Panjan and Joško Fišer for their kind assistance during indentation measurements. Rok Šulek and Niko Rozman (UM FS) are acknowledged for the vacuum melting and casting of alloys. We acknowledge Elettra, Sincrotrone Trieste, and the European Commission for reimbursement under EU contract RII3-CT-2004-506008 (IA-SFS), proposal 20090314. This work was also supported by the European Commision – Research Infractructure Action under the FP6 "European Integrated Activity of Excellence and Networking for Nano and Micro-Electronics Analysis". Project Number "0261334(RI3) ANNA".

References

[1] S.S. Ryu, H.T. Kim, H.J. Kim, S. Kim, J. Ceram. Soc. Jpn. 117 (2009) 811–814.
[2] O. Uzun, N. Guclu, U. Kolemen, O. Sahin, Mater. Chem. Phys. 112 (2008) 5–10.
[3] B.G. Yoo, K.W. Lee, J.I. Jang, J. Alloys Compd. 483 (2009) 136–138.
[4] Y.T. Chen, S.R. Jian, J. Alloys Compd. 481 (2009) 365–368.

[5] I. Zwierzak, M. Baleani, M. Viceconti, Proc. Inst. Mech. Eng. H: J. Eng. Med. 223 (2009) 913–918.
[6] Z.H. Xie, M.V. Swain, G. Swadener, P. Munroe, M. Hoffman, J. Biomech. 42 (2009) 1075–1080.
[7] N.K. Mukhopadhyay, A. Belger, P. Paufler, E. Uhrig, S. Bruhne, W. Assmus, J. Alloys Compd. 466 (2008) 160–164.
[8] W. Zhu, M.T.J. Fonteyn, J. Hughes, C. Pearce, Nanoindentation Study of Resin Impregnated Sandstone and Early-Age Cement Paste Specimens, Springer-Verlag, Berlin, 2009.
[9] N.K. Mukhopadhyay, P. Paufler, Int. Mater. Rev. 51 (2006) 209–245.
[10] N.K. Mukhopadhyay, A. Belger, P. Paufler, P. Gille, Philos. Mag. 86 (2006) 999–1005.
[11] S.N. Dub, Y.V. Milman, D.V. Lotsko, A.N. Belous, J. Mater. Sci. Lett. 20 (2001) 1043–1045.
[12] S.H. Kim, G.S. Song, E. Fleury, K. Chattopadhyay, W.T. Kim, D.H. Kim, Philos. Mag. A: Phys. Condens. Matter Struct. Defects Mech. Prop. 82 (2002) 1495–1508.
[13] A. Feuerbacher, A. Heggen, K. Urban, Mater. Sci. Eng. A: Struct. Mater. Prop. Microstruct. Process. 375–77 (2004) 84–89.
[14] J.M. Dubois, in: E. Belin-Ferré (Ed.), Basics of Thermodynamics and Phase Transitions in Complex Intermetallics, World Scientific Publishing Co., 2008, pp. 1–29.
[15] F. Zupanic, T. Boncina, N. Rozman, I. Anzel, W. Grogger, C. Gspan, F. Hofer, B. Markoli, Z. Kristall. 223 (2008) 735–738.
[16] J.A. Carrabine, J. Nucl. Mater. 8 (1963) 278–280.
[17] C.B. Shoemaker, Phys. Rev. B 38 (1988) 8511–8514.
[18] M. Jagodic, Z. Jaglicic, B. Grushko, S. Balanetskyy, J. Dolinsek, Z. Kristall. 224 (2009) 42–44.
[19] EN ISO 14577-1:2002, Metallic Materials—Instrumented Indentation Test for Hardness and Materials Parameters—Part I: Test Method, 2002.
[20] E. Giacometti, N. Baluc, J. Bonneville, J. Rabier, Scr. Mater. 41 (1999) 989–994.
[21] V.C. Srivastava, V. Uhlenwinkel, A. Schulz, H.W. Zoch, N.K. Mukhopadhyay, S.G. Chowdhury, Z. Kristall. 223 (2008) 711–715.
[22] U. Koster, W. Liu, H. Liebertz, M. Michel, J. Non-Cryst. Solids 153 (1993) 446–452.
[23] S.M. Lee, B.H. Kim, S.H. Kim, E. Fleury, W.T. Kim, D.H. Kim, Mater. Sci. Eng. A: Struct. Mater. Prop. Microstruct. Process. 294 (2000) 93–98.
[24] N.K. Mukhopadhyay, A. Belger, P. Paufler, D.H. Kim, Mater. Sci. Eng. A: Struct. Mater. Prop. Microstruct. Process. 449 (2007) 954–957.
[25] N.K. Mukhopadhyay, G.C. Weatherly, J.D. Embury, Mater. Sci. Eng. A: Struct. Mater. Prop. Microstruct. Process. 315 (2001) 202–210.